Gulf Journal of Mathematics
Vol 24, Issue 2 (2026) 1-14

ISSN: 2309-4966
https://doi.org/10.56947/tvacfg77

SPARSE LAGUERRE INVERSION OF BIVARIATE LAPLACE TRANSFORMS

MONTHER AL-MOMANI[1] and BAHA' ABUGHAZALEH[2*]

Abstract. We study sparse Laguerre recovery from bivariate Laplace samples. An exact aliasing identity yields a sharp stability estimate for scaled sample errors. Level balanced sampling preserves the mixed regularity truncation rate while reducing transform evaluations. A deterministic sampling lower bound leaves an iterated logarithmic gap in the recovery rate. An a priori stopping rule controls errors in unscaled samples. Six tests compare sparse and rectangular recovery and examine noise sensitivity. The practical advantage depends on the coefficient structure.

Keywords. Bivariate Laplace inversion, Laguerre approximation, hyperbolic cross, sparse recovery, regularization
2020 Mathematics Subject Classification. Primary 44A10; Secondary 65R10, 41A63

1. Introduction

Scaled Laguerre inversion [22] extends to multidimensional recovery with Fourier extraction [2, 18]. Parameter selection and method comparisons are discussed in [23, 12, 1]. Real axis inversion is exponentially ill posed [14]. Here complex nodes vary with the approximation level. Stability is measured in a specified norm on those samples.

Hyperbolic crosses reduce coefficient counts under mixed regularity [9, 13]. We combine this classical approximation with blockwise Fourier extraction. The contribution is a level balanced sampling rule with explicit aliasing and perturbation estimates. It reduces the sample cost from $O(2^J(J+1)^3)$ to $O(2^J(J+1)[1+\log(J+2)]^2)$ without changing the truncation rate. A deterministic sampling lower bound leaves an iterated logarithmic gap. A separate rule treats errors in the unscaled transform.

Related work treats Laguerre–Sobolev inversion [15], double transform calculus [8, 7, 5, 4, 3], nonlinear Sawi–Adomian decomposition [6] and local approximation for inversion and multiexponential smoothing [11, 10]. These works do not establish the sparse sampling bounds studied here. Our six tests retain unfavorable

Date: Received: Oct 6, 2026; Revised: Nov 5, 2026; Accepted: Nov 11, 2026.
* Corresponding author
© The Author(s) 2026. This article is licensed under a Creative Commons Attribution-NonCommercial-NoDerivatives 4.0 International License. To view a copy of the license, visit https://creativecommons.org/licenses/by-nc-nd/4.0/.

comparisons. Supplementary Material gives reference formulas and extended diagnostics.

2. Laguerre representation and mixed regularity

Let $H = L^2((0,\infty)^2;\mathbb{C})$ with Lebesgue measure. The transform of $f \in H$ is defined by

$$F(s,t) = \int_0^\infty \int_0^\infty e^{-sx-ty} f(x,y)\,dx\,dy, \qquad \Re s, \Re t > 0. \tag{2.1}$$

The Cauchy–Schwarz inequality ensures absolute convergence with $|F(s,t)| \le \|f\|_H / (2\sqrt{\Re s \Re t})$. Fix $a, b > 0$ and set

$$\varphi_n^a(x) = \sqrt{2a}\, e^{-ax} L_n(2ax), \qquad \Phi_{nm}(x,y) = \varphi_n^a(x)\varphi_m^b(y). \tag{2.2}$$

Here L_n is the ordinary Laguerre polynomial. The products Φ_{nm} form an orthonormal basis of H [22, 2, 18]. The scales a, b are prescribed positive parameters [23].

Proposition 2.1. *With $c_{nm} = \langle f, \Phi_{nm}\rangle_H$ define*

$$s_a(z) = a\frac{1+z}{1-z}, \qquad G(z,w) = \frac{2\sqrt{ab}}{(1-z)(1-w)} F(s_a(z), s_b(w)). \tag{2.3}$$

Then

$$G(z,w) = \sum_{n,m\ge 0} c_{nm} z^n w^m, \qquad \|f\|_H^2 = \sum_{n,m\ge 0} |c_{nm}|^2 = \|G\|^2_{H^2(\mathbb{D}^2)}. \tag{2.4}$$

On each compact sub-bidisc the power series is absolutely convergent.

Proof. Direct integration yields

$$\int_0^\infty e^{-sx} \varphi_n^a(x)\,dx = \frac{\sqrt{2a}}{s+a}\left(\frac{s-a}{s+a}\right)^n.$$

Apply the identity first to a finite sum of Laguerre functions. Laplace evaluation is a bounded functional on H, so the identity extends by H convergence. For $|z|, |w| < 1$, Cauchy–Schwarz bounds the absolute series by $\|c\|_{\ell^2} / \sqrt{(1-|z|^2)(1-|w|^2)}$. Orthogonality on circles and monotone convergence of the squared coefficients establish the last equality in (2.4). □

Define disjoint index blocks by

$$I_0 = \{0\}, \qquad I_\ell = \{2^{\ell-1}, \dots, 2^\ell - 1\} \quad (\ell \ge 1), \qquad \lambda(n) = \ell \quad (n \in I_\ell). \tag{2.5}$$

For $r > 0$, the mixed spectral space $\mathcal{H}^r$ is equipped with

$$\|f\|^2_{\mathcal{H}^r} = \sum_{n,m\ge 0} 2^{2r(\lambda(n)+\lambda(m))} |c_{nm}|^2. \tag{2.6}$$

Membership in $\mathcal{H}^r$ is an additional regularity assumption [13, 9].

For comparison with a differential scale, let A_a be the nonnegative self-adjoint operator defined spectrally by $A_a \varphi_n^a = a(2n+1)\varphi_n^a$. On finite Laguerre sums it

agrees with $-(xv')' + a^2xv$. Set $H_a = (A_a + aI)/(2a)$ and define powers spectrally. The inequalities $n+1 \le 2^{\lambda(n)} \le 2(n+1)$ give

$$\|(H_a^r \otimes H_b^r)f\|_H \le \|f\|_{\mathcal{H}^r} \le 2^{2r} \|(H_a^r \otimes H_b^r)f\|_H . \tag{2.7}$$

No boundary-domain characterization of fractional powers is needed below.

3. Sparse projection and its approximation benchmark

Let

$$\begin{aligned} \mathcal{B}_J &= \{(\ell,k) \in \mathbb{N}_0^2 : \ell + k \le J\}, \qquad \Lambda_J = \bigcup_{(\ell,k)\in\mathcal{B}_J} I_\ell \times I_k, \\ & \qquad\qquad P_J f = \sum_{(n,m)\in\Lambda_J} c_{nm}\Phi_{nm}. \end{aligned} \tag{3.1}$$

The number of blocks and retained coefficients are

$$K_J = \frac{(J+1)(J+2)}{2}, \qquad d_0 = 1, \qquad d_J = 2^{J-1}(J+2) \quad (J \ge 1). \tag{3.2}$$

Indeed $|I_0| = 1$ and $|I_\ell| = 2^{\ell-1}$ for $\ell \ge 1$. For $j \ge 1$ the shell $\lambda(n) + \lambda(m) = j$ contains $(j+3)2^{j-2}$ indices. Summing the shells proves (3.2).

Theorem 3.1. *Let $\mathcal{E}_r(M) = \{f : \|f\|_{\mathcal{H}^r} \le M\}$. Then*

$$\sup_{f\in\mathcal{E}_r(M)} \|f - P_J f\|_H = M2^{-r(J+1)}. \tag{3.3}$$

Among bounded linear operators $T : \mathcal{H}^r \to H$ of rank at most d_J, no smaller worst-case error is possible.

Proof. Every omitted index has $\lambda(n) + \lambda(m) \ge J+1$. Parseval gives

$$\|f - P_J f\|_H^2 \le 2^{-2r(J+1)} \sum_{(n,m)\notin\Lambda_J} 2^{2r(\lambda(n)+\lambda(m))} |c_{nm}|^2.$$

A single coefficient of size $M2^{-r(J+1)}$ on the first omitted shell gives equality. For the rank assertion, take the span of the d_J retained basis functions and one function from that shell. The restriction of T has a nonzero kernel vector v in this (d_J+1) dimensional space. Normalize it by $\|v\|_H = 1$. Its $\mathcal{H}^r$ norm is at most $2^{r(J+1)}$. Thus $f = M2^{-r(J+1)}v$ belongs to $\mathcal{E}_r(M)$ and $\|f - Tf\|_H = M2^{-r(J+1)}$. □

The rank statement is the standard diagonal-ellipsoid argument. It concerns exact coefficient information and does not assert optimality among algorithms using a given number of transform samples.

4. Blockwise recovery from transform samples

Fix $\kappa > 0$ and an integer $q \ge 1$. For each $\ell \ge 0$ define

$$N_\ell = 2^\ell, \qquad L_\ell = qN_\ell, \qquad \rho_\ell = e^{-\kappa/N_\ell}, \qquad z_{\ell,j} = \rho_\ell e^{2\pi ij/L_\ell} \quad (0 \le j < L_\ell). \tag{4.1}$$

On block (ℓ, k) sample $F(s_a(z_{\ell,j}), s_b(z_{k,h}))$ and form the scaled array G in (2.3). For $(n, m) \in I_\ell \times I_k$ set

$$\widetilde{c}_{nm} = \frac{\rho_\ell^{-n}\rho_k^{-m}}{L_\ell L_k} \sum_{j=0}^{L_\ell-1} \sum_{h=0}^{L_k-1} G(z_{\ell,j}, z_{k,h}) e^{-2\pi i(nj/L_\ell + mh/L_k)}. \tag{4.2}$$

Each coefficient is taken from exactly one block. The approximation is

$$Q_{J,q} f = \sum_{(n,m)\in\Lambda_J} \widetilde{c}_{nm} \Phi_{nm}. \tag{4.3}$$

The circles depend on the block level. The retained exponents satisfy

$$1 \le \rho_\ell^{-n}\rho_k^{-m} < e^{2\kappa}. \tag{4.4}$$

Root-of-unity coefficient recovery is a classical contour-quadrature construction [21]. The block restriction in (4.2) is what gives the sparse sample count.

Proposition 4.1. *Counting a repeated evaluation on different block arrays separately,*

$$S_{J,q} = \sum_{\ell+k\le J} L_\ell L_k = q^2\{1 + J2^{J+1}\}. \tag{4.5}$$

Two-dimensional FFTs require $O(S_{J,q}\log(q2^J))$ arithmetic operations. Processing one block at a time requires $O(q^2 2^J + d_J)$ storage when retained coefficients are stored sparsely.

Proof. There are $j+1$ blocks with $\ell+k=j$, so the sample count is $q^2\sum_{j=0}^{J}(j+1)2^j$. The sum equals $q^2(1+J2^{J+1})$. Each FFT acts on an array of at most $q^2 2^J$ entries. Summing the FFT costs and retaining only d_J coefficients gives the claims. □

4.1. **Aliasing.**

Lemma 4.2. *With exact input samples, for $(n, m) \in I_\ell \times I_k$,*

$$\widetilde{c}_{nm} - c_{nm} = \sum_{\substack{p,h\ge 0\\ p+h>0}} c_{n+pL_\ell, m+hL_k}\, e^{-\kappa q(p+h)}. \tag{4.6}$$

If $\eta = e^{-\kappa q}$ and

$$B_q = \sqrt{(1-\eta^2)^{-2} - 1}, \tag{4.7}$$

then

$$\|Q_{J,q} f - P_J f\|_H \le \sqrt{K_J}\, B_q\, \|f\|_H. \tag{4.8}$$

Proof. The absolutely convergent series (2.4) may be substituted in (4.2). The two finite Fourier sums vanish unless the coefficient indices have residues n and m modulo L_ℓ and L_k. Since $n < L_\ell$ and $m < L_k$, all surviving offsets are nonnegative. This proves (4.6). Cauchy–Schwarz gives

$$|\widetilde{c}_{nm} - c_{nm}|^2 \le B_q^2 \sum_{p+h>0} |c_{n+pL_\ell, m+hL_k}|^2.$$

The residue classes are disjoint within each block. Their squared sums are at most $\|f\|_H^2$. Summing over the K_J output blocks proves (4.8). Residue classes from different blocks need not be disjoint, which accounts for the factor $\sqrt{K_J}$. □

4.2. **Perturbed scaled samples.** Suppose block (ℓ, k) supplies $G + E^{\ell k}$. Define its discrete RMS error and the combined data norm by

$$\epsilon_{\ell k}^2 = \frac{1}{L_\ell L_k} \sum_{j,h} |E_{jh}^{\ell k}|^2, \qquad \epsilon_J^2 = \sum_{\ell+k \le J} \epsilon_{\ell k}^2. \tag{4.9}$$

Denote the noisy reconstruction by $Q_{J,q}^E f$.

Theorem 4.3. *For arbitrary complex perturbations,*

$$\left\| Q_{J,q}^E f - Q_{J,q} f \right\|_H \le e^{2\kappa} \epsilon_J. \tag{4.10}$$

If $f \in \mathcal{E}_r(M)$, then

$$\left\| f - Q_{J,q}^E f \right\|_H \le \left[M^2 2^{-2r(J+1)} + \left(M\sqrt{K_J} B_q + e^{2\kappa} \epsilon_J \right)^2 \right]^{1/2}. \tag{4.11}$$

The constant $e^{2\kappa}$ in (4.10) cannot be reduced uniformly over all J in the data norm (4.9).

Proof. Discrete Parseval for the Fourier coefficients normalized by $L_\ell L_k$ gives the sum of all squared Fourier coefficients of $E^{\ell k}$ as $\epsilon_{\ell k}^2$. Selecting the desired residues can only decrease it. The division by the radii amplifies each selected coefficient by less than $e^{2\kappa}$. The blocks have disjoint output indices, giving (4.10). The omitted tail is orthogonal to the retained coefficient error. Combine this fact with Theorem 3.1, Lemma 4.2 and the triangle inequality to obtain (4.11).

For sharpness choose a single block $\ell = k$, $J = 2\ell$, and perturb only that block by $E_{jh} = \epsilon e^{2\pi i (nj/L_\ell + mh/L_\ell)}$ with $n = m = 2^\ell - 1$. Its RMS is ϵ and the output consists of one coefficient of magnitude $\epsilon e^{2\kappa(1-2^{-\ell})}$. Letting $\ell \to \infty$ gives the asserted uniform lower bound. □

Stability in (4.10) concerns scaled transform data and the H norm. It is not uniform stability for unweighted errors in F, nor does it imply a uniform pointwise error bound on the unbounded quadrant. In particular, it does not remove the ill-conditioning of real-axis Laplace inversion studied in [14]. Here complex sampling nodes vary with the approximation level. Smoothing multiexponential data is a distinct approximation task, as illustrated in [10].

5. Oversampling and regularization

Corollary 5.1. *Let $f \in \mathcal{E}_r(M)$ with $r, M > 0$. Choose*

$$q_J = \max\left\{1, \left\lceil \frac{r(J+1)\log 2 + \log(4\sqrt{K_J})}{\kappa} \right\rceil \right\}. \tag{5.1}$$

With exact samples,

$$\|f - Q_{J,q_J} f\|_H \le \sqrt{2} M 2^{-r(J+1)}, \qquad S_{J,q_J} = O(2^J (J+1)^3). \tag{5.2}$$

Consequently, along these levels, $\|f - Q_{J,q_J} f\|_H = O(M S_{J,q_J}^{-r} (\log S_{J,q_J})^{3r})$.

Proof. For $0 \le \eta \le 1/2$, (4.7) gives $B_q \le 2\eta$. The choice (5.1) implies $\sqrt{K_J} B_{q_J} \le 2^{-r(J+1)}/2$. Equation (4.11) proves the stated, slightly relaxed error bound. For fixed $r, \kappa > 0$, $q_J = \Theta(J+1)$. Equation (4.5) gives the sample bound and its inversion. □

For a square projection with $0 \le n, m < 2^J$, the same class has worst-case tail $M2^{-r(J+1)}$, since an omitted axis coefficient attains that value. One tensor contour grid needs $q_J^2 4^J$ samples. This comparison concerns worst-case mixed regularity. Individual functions may strongly favor the square projection.

5.1. **Level-balanced sampling.** The uniform oversampling rule spends the same q_J on every block, although mixed regularity suppresses high-level coefficients. We instead assign

$$q_{J,j} = \max\left\{1, \left\lceil \frac{r(J+1-j)\log 2 + \log(4\sqrt{K_J})}{\kappa} \right\rceil \right\}, \qquad 0 \le j \le J. \tag{5.3}$$

On block (ℓ, k), use $L_\ell = q_{J,\ell+k} 2^\ell$ and $L_k = q_{J,\ell+k} 2^k$ in (4.2); the radii are unchanged. Write the resulting operator as $\mathcal{Q}_J$.

Lemma 5.2. *Let $f \in \mathcal{E}_r(M)$ and let $A_{\ell k}$ be the coefficient error on $I_\ell \times I_k$ with oversampling q. Then*

$$\|A_{\ell k}\|_{\ell^2} \le M 2^{-r(\ell+k)} B_q. \tag{5.4}$$

Consequently, arbitrary block choices $q_{\ell k} \ge 1$ satisfy

$$\|\mathcal{Q}_J f - P_J f\|_H^2 \le M^2 \sum_{\ell+k \le J} 2^{-2r(\ell+k)} B_{q_{\ell k}}^2. \tag{5.5}$$

Proof. Every source index in (4.6) obeys $\lambda(n + pL_\ell) \ge \ell$ and $\lambda(m + hL_k) \ge k$. In the proof of Lemma 4.2, the squared source coefficients on a block therefore sum to at most $2^{-2r(\ell+k)} M^2$. The residue classes remain disjoint within that block. Apply Cauchy–Schwarz as before and sum the squared errors over the disjoint output blocks. □

Theorem 5.3. *For $f \in \mathcal{E}_r(M)$, $r, M, \kappa > 0$, rule (5.3) gives*

$$\left\|f - \mathcal{Q}_J^E f\right\|_H \le \left[M^2 2^{-2r(J+1)} + \left(\tfrac{1}{2} M 2^{-r(J+1)} + e^{2\kappa} \epsilon_J\right)^2\right]^{1/2}, \tag{5.6}$$

$$S_J^{\mathrm{bal}} = \sum_{j=0}^{J} (j+1) 2^j q_{J,j}^2 = \Theta\left(2^J (J+1)[1 + \log(J+2)]^2\right). \tag{5.7}$$

The constants in Θ may depend on r and κ. With exact data and $S = S_J^{\mathrm{bal}}$,

$$\|f - \mathcal{Q}_J f\|_H = O\left(M S^{-r} [\log(S+1)]^r [1 + \log\log(S+e)]^{2r}\right). \tag{5.8}$$

Proof. For $j = \ell + k$, the rule gives $e^{-\kappa q_{J,j}} \le 2^{-r(J+1-j)}/(4\sqrt{K_J}) < 1/2$. Since $B_q \le 2e^{-\kappa q}$ in this range,

$$2^{-rj} B_{q_{J,j}} \le \frac{2^{-r(J+1)}}{2\sqrt{K_J}}.$$

Equation (5.5) bounds the total alias error by $M2^{-r(J+1)}/2$. The noise proof of Theorem 4.3 uses only the unchanged radii and is valid for every block size. Orthogonality of the omitted tail proves (5.6).

Put $A_J = 1 + \log(J+2)$. Equation (5.3) implies $q_{J,j} \le C_{r,\kappa}(J - j + A_J)$. With $h = J - j$,

$$S_J^{\mathrm{bal}} \le C_{r,\kappa}^2 2^J (J+1) \sum_{h=0}^{\infty} 2^{-h}(h + A_J)^2 \le C'_{r,\kappa} 2^J (J+1) A_J^2.$$

The last shell alone gives the matching lower bound because $q_{J,J} \ge c_{r,\kappa} A_J$. Thus $\log(S+1) = \Theta(J+1)$ and $1 + \log\log(S+e) = \Theta(A_J)$. Rearranging (5.7) and applying (5.6) with $E = 0$ proves (5.8). □

The coefficient set is unchanged. The improvement is in transform samples, from $O(2^J J^3)$ to $O(2^J J(\log J)^2)$ as $J \to \infty$. This is a level-dependent contour construction, not the classical Smolyak combination formula [19, 16].

Theorem 5.4. *Work over the complex Hilbert space H. Let a deterministic algorithm use at most S complex evaluations of F in the product of right half-planes. Its nodes may depend on previously observed values, and its output may be nonlinear. If L is the smallest integer with $d_L > S$, then*

$$\sup_{f \in \mathcal{E}_r(M)} \|f - \mathcal{A}_S(F)\|_H \ge M2^{-rL} \ge c_r M \left(\frac{\log(S+1)}{S} \right)^r, \qquad S \ge 2. \tag{5.9}$$

Proof. Run the algorithm on zero data and fix the at most S nodes on that path. Their evaluations are linear functionals on the d_L dimensional space $\operatorname{span}\{\Phi_{nm} : (n,m) \in \Lambda_L\}$. Their common kernel contains an H-unit vector v. Its mixed norm is at most 2^{rL}. The inputs $\pm f_* = \pm M2^{-rL} v$ lie in $\mathcal{E}_r(M)$ and produce exactly the same zero-data path, including all adaptive choices. If u is the common output, the triangle inequality yields $\max\{\|f_* - u\|_H, \|-f_* - u\|_H\} \ge \|f_*\|_H$. Finally $d_{L-1} \le S < d_L$ and (3.2) imply $2^L \asymp S/\log(S+1)$ for $S \ge 2$, proving the last inequality. □

Thus the upper and lower rates differ by at most an iterated-logarithmic factor for this information model. Exact sampling optimality is not asserted. For real-valued inputs a complex sample imposes at most two real constraints; using $d_L > 2S$ gives the same order of lower bound.

Block-list implementation. For each (ℓ, k) compute (5.3), sample and scale F, apply the normalized two-dimensional FFT, and retain only $I_\ell \times I_k$. Store that coefficient block and release its sampling array before the next block. This uses d_J coefficient entries and at most $\max_j q_{J,j}^2 2^j$ sampling entries. Physical values are evaluated by summing the stored blocks with the Laguerre recurrence.

5.2. **Errors in the unscaled transform.** Let the measured values be $F + \Delta F^{\ell k}$ with RMS error at most $\delta_{\ell k}$ on each block. Multiplication in (2.3) implies

$$\epsilon_{\ell k} \le W_{\ell k} \delta_{\ell k}, \qquad W_{\ell k} = \frac{2\sqrt{ab}}{(1-\rho_\ell)(1-\rho_k)}. \tag{5.10}$$

The computable data contribution in (4.11) is therefore bounded by

$$e^{2\kappa}\left(\sum_{\ell+k\le J} W_{\ell k}^2\delta_{\ell k}^2\right)^{1/2}. \tag{5.11}$$

Theorem 5.5. *Let $f\in\mathcal{E}_r(M)$ with $r,M>0$. Assume $\delta_{\ell k}\le\delta$ and $0<\delta\le M$. With $q=q_J$,*

$$\left\|f-Q^E_{J,q_J}f\right\|_H \le \sqrt{2}M2^{-r(J+1)}+C_{a,b,\kappa}\delta\sqrt{J+1}\,2^J,\quad C_{a,b,\kappa}=\frac{4\sqrt{ab}e^{4\kappa}}{\sqrt{3}\kappa^2}. \tag{5.12}$$

Choose the largest nonnegative $J=J_\delta$ satisfying

$$2^{(r+1)J}\sqrt{J+1}\le M/\delta. \tag{5.13}$$

For fixed r,a,b,κ, as $\delta/M\to 0$,

$$\left\|f-Q^E_{J_\delta,q_{J_\delta}}f\right\|_H = O\left(M^{1/(r+1)}\delta^{r/(r+1)}[1+\log(M/\delta)]^{r/(2r+2)}\right). \tag{5.14}$$

Proof. Since $1-e^{-u}\ge ue^{-\kappa}$ for $0<u\le\kappa$, $W_{\ell k}\le 2\sqrt{ab}e^{2\kappa}2^{\ell+k}/\kappa^2$. Also

$$\sum_{\ell+k\le J}4^{\ell+k}=\sum_{j=0}^{J}(j+1)4^j\le\frac{4}{3}(J+1)4^J.$$

Combine (5.11) and Corollary 5.1 to obtain (5.12). The level in (5.13) exists because $\delta\le M$. At that level the noise term is at most $C_{a,b,\kappa}M2^{-rJ}$. Maximality gives $2^{(r+1)(J+1)}\sqrt{J+2}>M/\delta$ and hence

$$M2^{-rJ}<2^rM^{1/(r+1)}\delta^{r/(r+1)}(J+2)^{r/(2r+2)}.$$

Finally $(r+1)J\log 2\le\log(M/\delta)$ proves (5.14). □

The constants require an upper bound M and regularity index r. The same bound and stopping rule hold for $\mathcal{Q}^E_J$, by Theorem 5.3; the weights in (5.10) do not depend on q. The selection rule is an a priori regularization rule, not an estimate of unknown smoothness from noisy observations. Relative transform noise and roundoff must first be converted to a bound on $\delta_{\ell k}$.

5.3. **Anisotropic block sets.** For $r_1,r_2>0$ replace (2.6) by weights $2^{2(r_1\lambda(n)+r_2\lambda(m))}$ and retain blocks $\mathcal{B}_T=\{(\ell,k):r_1\ell+r_2k\le T\}$. Let $\omega_T=\min_{(\ell,k)\notin\mathcal{B}_T}(r_1\ell+r_2k)$. The same proofs give the tail $M2^{-\omega_T}$, alias bound $M\sqrt{|\mathcal{B}_T|}B_q$, scaled-noise constant $e^{2\kappa}$ and sample count

$$S_T=q^2\sum_{(\ell,k)\in\mathcal{B}_T}2^{\ell+k}. \tag{5.15}$$

We use $r_1=r_2=1$ in the initial comparisons and $(r_1,r_2)=(1,2)$ in the additional anisotropic test.

6. Numerical tests

All tests use $a = b = \kappa = 1$ unless stated otherwise. The initial runs use $q = \max\{4, q_J\}$ with $r = 1$. The solver receives complex transform samples only. Reference coefficients are calculated separately. Computations use Python 3.12.14 with NumPy 2.5.3 in binary64 arithmetic on an Intel Core i5-1135G7 processor under Windows 11. The initial output is dense. Balanced sampling uses the block list implementation described above. Every block evaluation is counted even if its node occurs in another block.

6.1. **Transform pairs and error measurement.** The first four tests are

$$f_A(x,y) = e^{-x-2y} + 0.6e^{-4x-y/2} + 0.3e^{-3x/2-3y},$$

$$F_A(s,t) = \frac{1}{(s+1)(t+2)} + \frac{0.6}{(s+4)(t+1/2)} + \frac{0.3}{(s+3/2)(t+3)}, \tag{6.1}$$

$$f_B(x,y) = e^{-x-y} I_0(2\sqrt{\theta xy}), \quad F_B(s,t) = \frac{1}{(s+1)(t+1)-\theta}, \quad \theta = 0.8, \tag{6.2}$$

$$f_C(x,y) = \frac{2^{\beta+\gamma+1} x^\beta y^\gamma e^{-x-y}}{\Gamma(\beta+1)\Gamma(\gamma+1)}, \quad F_C(s,t) = \frac{2^{\beta+\gamma+1}}{(s+1)^{\beta+1}(t+1)^{\gamma+1}}, \tag{6.3}$$

$$f_D(x,y) = \frac{2}{1-\zeta} e^{-\frac{1+\zeta}{1-\zeta}(x+y)} I_0\left(\frac{4\sqrt{\zeta xy}}{1-\zeta}\right), \quad \zeta = 0.8,$$

$$F_D(s,t) = \frac{2}{(s+1)(t+1) - \zeta(s-1)(t-1)}. \tag{6.4}$$

Here I_0 is the modified Bessel function. Test C uses $(\beta, \gamma) = (0.6, 0.9)$ with principal powers in the right half-plane. Its coefficients are $(-1)^{n+m}\binom{\beta}{n}\binom{\gamma}{m}$ and $f_C \in \mathcal{H}^r$ for $r < 1.1$. Test D has $c_{nm} = \zeta^n \mathbf{1}_{\{n=m\}}$ and concentrates coefficient energy on the diagonal.

The error is evaluated from Parseval as

$$E^2 = \sum_{(n,m)\notin\Lambda} |c_{nm}|^2 + \sum_{(n,m)\in\Lambda} |c_{nm} - \widetilde{c}_{nm}|^2. \tag{6.5}$$

Tests A, B and D use 512×512 reference arrays with analytic tail bounds. Test C uses its exact squared norm. Supplementary Section S1 gives the coefficient formulas and tail estimates. These estimates do not enclose floating point roundoff.

6.2. **Sparse and rectangular recovery.** The rectangle uses $N = \lfloor \sqrt{S_{J,q}}/q \rfloor$, one $qN \times qN$ grid and radius $e^{-1/N}$ in both coordinates. Its N^2 coefficients require no more samples than the sparse approximation. This is a tensor Laguerre–FFT baseline based on [2]. Table 1 and Figure 1 show an advantage for the cross at the higher budgets for C. Rectangles are more accurate for A, B and D.

Table 1. Sparse and rectangular reconstructions at comparable transform-sample budgets. E is the global L^2 error. Both use the same q_J.

Test	J	q_J	d_J	S_J	N	S_{rect}	E_{sparse}	E_{rect}
A	3	6	20	1764	7	1764	1.301×10^{-2}	5.975×10^{-3}
A	5	8	112	20544	17	18496	5.233×10^{-4}	3.591×10^{-5}
A	7	9	576	145233	42	142884	9.445×10^{-7}	1.021×10^{-10}
B	3	6	20	1764	7	1764	1.877×10^{-1}	2.813×10^{-2}
B	5	8	112	20544	17	18496	6.562×10^{-2}	4.232×10^{-4}
B	7	9	576	145233	42	142884	9.647×10^{-3}	1.416×10^{-8}
C	3	6	20	1764	7	1764	5.091×10^{-2}	3.335×10^{-2}
C	5	8	112	20544	17	18496	9.335×10^{-3}	1.155×10^{-2}
C	7	9	576	145233	42	142884	1.949×10^{-3}	4.125×10^{-3}
D	3	6	20	1764	7	1764	1.067×10^{0}	3.495×10^{-1}
D	5	8	112	20544	17	18496	6.827×10^{-1}	3.753×10^{-2}
D	7	9	576	145233	42	142884	2.796×10^{-1}	1.418×10^{-4}

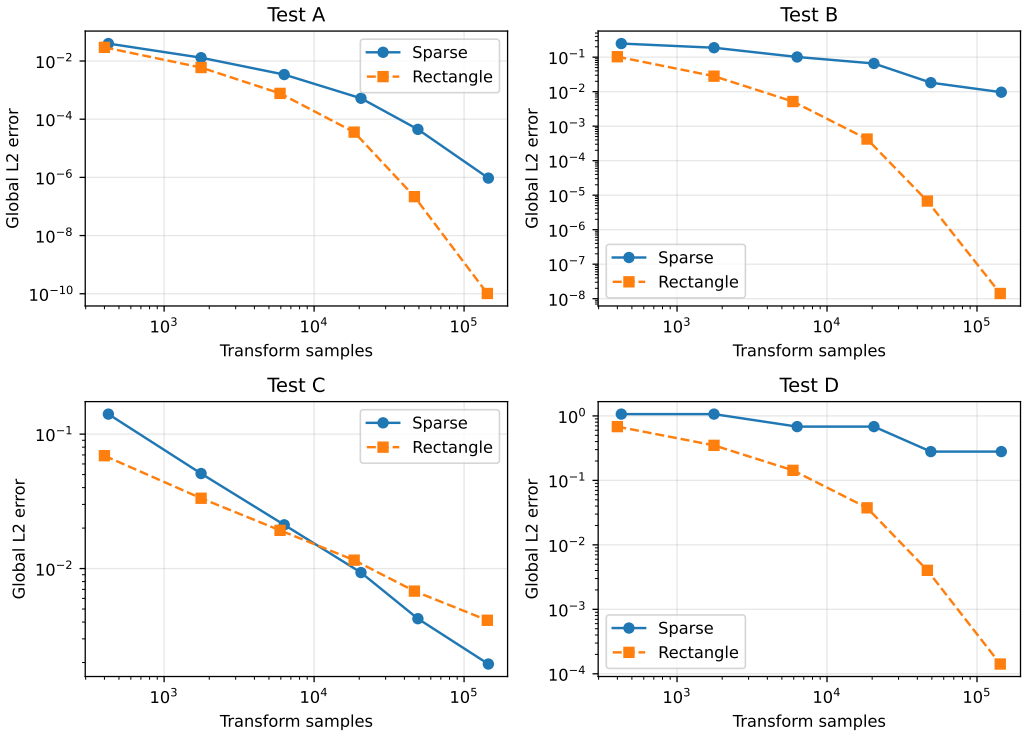


Fig. 1. Global error against complex transform evaluations for A–D. Solid curves: sparse recovery. Dashed curves: rectangular recovery.

7. Balanced sampling

For the nonseparable tests E and F let

$$F_{\beta,\gamma,\theta}(s,t) = \frac{2^{\beta+\gamma+1}}{(s+1)^{\beta+1}(t+1)^{\gamma+1}} \left(1 - \theta \frac{s-1}{s+1}\frac{t-1}{t+1}\right)^{-1}, \tag{7.1}$$

$$c_{nm} = \sum_{h=0}^{\min(n,m)} \theta^h u_{n-h} v_{m-h}, \quad u_n = (-1)^n \binom{\beta}{n}, \quad v_m = (-1)^m \binom{\gamma}{m}. \tag{7.2}$$

Test E uses $(\beta,\gamma,\theta) = (0.6, 0.9, 0.2)$ and F uses $(0.6, 1.6, 0.2)$. Their coefficient matrices have infinite rank and their mixed norm is finite for $r_1 < \beta + 1/2$ and $r_2 < \gamma + 1/2$. Supplementary Section S2 proves these statements and bounds the omitted tails of the 2048×2048 reference arrays. The squared tail bounds are 5.07×10^{-9} for E and 1.06×10^{-8} for F. The relative widths of the error intervals in Table 2 are below 0.37%. They are evaluated in binary64 without directed rounding.

Table 2 compares uniform and balanced sampling on the same cross. At each balanced budget the rectangular baseline tests $q = 2, \ldots, 9$ with $N = \lfloor \sqrt{S_b}/q \rfloor$. The result with the smallest reference error is reported. This oracle favors the baseline. The balanced solver does not use reference errors. At $J = 8$ balancing reduces samples from 409700 to 95364 with little change in the cross error. It does not consistently beat the tuned rectangle.

Table 2. Uniform and level-balanced recovery. E_b^+ and E_u^+ are upper endpoints of reference-tail error intervals. The rectangular baseline is oracle-tuned over $q = 2, \ldots, 9$ within the balanced budget.

Test	J	S_b	S_u	E_b^+	E_u^+	E_{rect}^+
C	4	2573	6321	2.115×10^{-2}	2.115×10^{-2}	7.426×10^{-3}
C	6	16908	49216	4.237×10^{-3}	4.237×10^{-3}	2.533×10^{-3}
C	8	95364	409700	9.030×10^{-4}	9.030×10^{-4}	9.719×10^{-4}
E	4	2573	6321	2.170×10^{-2}	2.170×10^{-2}	6.794×10^{-3}
E	6	16908	49216	3.976×10^{-3}	3.976×10^{-3}	2.323×10^{-3}
E	8	95364	409700	8.397×10^{-4}	8.397×10^{-4}	8.932×10^{-4}
F	4	2573	6321	4.297×10^{-2}	4.297×10^{-2}	9.479×10^{-3}
F	6	16908	49216	6.475×10^{-3}	6.475×10^{-3}	3.251×10^{-3}
F	8	95364	409700	1.387×10^{-3}	1.387×10^{-3}	1.252×10^{-3}

Figure 2 also shows test A with raw transform noise. Each noise level uses five independent complex perturbations with block RMS δ and seed 924731. Rule (5.13) uses the proven prior bound $M_A = 3.958479867826896$ with $r = 1$. The reference oracle minimizes mean error over $0 \le J \le J_\delta + 1$. The bound and individual results are given in Supplementary Section S6. The prescribed level is not always the oracle level.

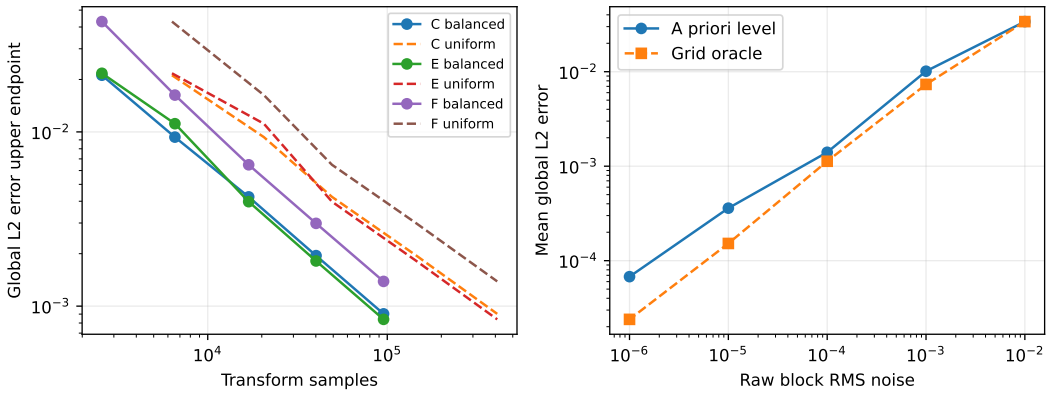


Fig. 2. Left: balanced and uniform sampling for C, E and F. Right: raw-noise test A with the prior stopping level and a reference oracle.

The scales a, b and contour parameter κ remain prescribed inputs. Supplementary Figure S3 tests all 27 choices in $\{0.5, 1, 2\}^3$. Its budgets vary with κ. Automatic selection from noisy transform values is not supplied by the present analysis. Supplementary Sections S3–S7 also retain the aliasing and perturbation sweeps, timings, anisotropic tests and storage measurements. The independent Gaver–Stehfest comparison [20, 1, 17] gives smaller sampled pointwise errors at high orders with higher precision. This pointwise task differs from reusable global approximation.

8. Conclusion

Level balanced sampling retains the sparse Laguerre truncation rate with fewer evaluations than uniform oversampling. The scaled noise constant is sharp in the stated data norm. The upper recovery rate differs from the deterministic sampling lower bound by an iterated logarithmic factor. The tests show that rectangles can be more accurate for individual functions. The raw noise stopping rule requires prior regularity and size bounds. Automatic scale selection and a smaller sampling gap remain open.

Disclosure of AI-assisted tools

AI-assisted tools were used during manuscript preparation. The authors are responsible for reviewing and verifying the content and for the final version.

References

[1] Abate, J., & Whitt, W. (2006). A unified framework for numerically inverting Laplace transforms. *INFORMS Journal on Computing*, *18*(4), 408–421. https://doi.org/10.1287/ijoc.1050.0137

[2] Abate, J., Choudhury, G. L., & Whitt, W. (1998). Numerical inversion of multidimensional Laplace transforms by the Laguerre method. *Performance Evaluation*, *31*(3–4), 229–243. https://doi.org/10.1016/S0166-5316(97)00002-3

[3] Abu Awwad, R. R., Al-Momani, M., Abughazaleh, B., Jaradat, A., & Farah, A. (2025). The conformable double Laplace-Sawi transform. *European Journal of Pure and Applied Mathematics*, *18*(2), Article 6034. https://doi.org/10.29020/nybg.ejpam.v18i2.6034

[4] Abu Awwad, R. R., Al-Momani, M., Jaradat, A., Abughazaleh, B., & Al-Natoor, A. (2025). The double ARA-Sawi transform. *European Journal of Pure and Applied Mathematics*, *18*(1), Article 5807. https://doi.org/10.29020/nybg.ejpam.v18i1.5807

[5] Abughazaleh, B., Amleh, M. A., Al-Natoor, A., & Saadeh, R. (2024). Double Mellin-ARA transform. In A. Burqan, R. Saadeh, A. Qazza, O. Y. Ababneh, J. C. Cortés, K. Diethelm, & D. Zeidan (Eds.), *Mathematical analysis and numerical methods* (Springer Proceedings in Mathematics & Statistics, Vol. 466, pp. 383–394). Springer. https://doi.org/10.1007/978-981-97-4876-1_26

[6] Al-Momani, M., & Abughazaleh, B. (2026a). Analytical solutions of nonlinear partial differential equations using the double Sawi–Adomian decomposition method. *Journal of Applied Mathematics*, *2026*(1), Article 2272559. https://doi.org/10.1155/jama/2272559

[7] Al-Momani, M., & Abughazaleh, B. (2026b). Double ARA–Shehu transform for partial integro-differential equations. *Gulf Journal of Mathematics*, *24*(1), 1–11. https://doi.org/10.56947/hg505s15

[8] Al-Momani, M., Jaradat, A., & Abughazaleh, B. (2025). Double Laplace-Sawi transform. *European Journal of Pure and Applied Mathematics*, *18*(1), Article 5619. https://doi.org/10.29020/nybg.ejpam.v18i1.5619

[9] Bungartz, H.-J., & Griebel, M. (2004). Sparse grids. *Acta Numerica*, *13*, 147–269. https://doi.org/10.1017/S0962492904000182

[10] Campagna, R., Conti, C., & Cuomo, S. (2019). Smoothing exponential-polynomial splines for multiexponential decay data. *Dolomites Research Notes on Approximation*, *12*(1), 86–100. https://doi.org/10.14658/PUPJ-DRNA-2019-1-9

[11] Campagna, R., Cuomo, S., & Bayona, V. (2020). Using local PHS+poly approximations for Laplace Transform Inversion by Gaver-Stehfest algorithm. *Dolomites Research Notes on Approximation*, *13*(1), 55–64. https://doi.org/10.14658/PUPJ-DRNA-2020-1-7

[12] Davies, B., & Martin, B. (1979). Numerical inversion of the Laplace transform: a survey and comparison of methods. *Journal of Computational Physics*, *33*(1), 1–32. https://doi.org/10.1016/0021-9991(79)90025-1

[13] Dũng, D., Temlyakov, V., & Ullrich, T. (2018). *Hyperbolic cross approximation*. Birkhäuser. https://doi.org/10.1007/978-3-319-92240-9

[14] Epstein, C. L., & Schotland, J. (2008). The bad truth about Laplace's transform. *SIAM Review*, *50*(3), 504–520. https://doi.org/10.1137/060657273

[15] Fuentes, E., Riscanevo, L. E., & Silva, M. A. (2026). Inverse Laplace transform and spectral method based on Laguerre-Sobolev-type polynomials. *AIMS Mathematics*, *11*(7), 20364–20388. https://doi.org/10.3934/math.2026827

[16] Gerstner, T., & Griebel, M. (1998). Numerical integration using sparse grids. *Numerical Algorithms*, *18*(3–4), 209–232. https://doi.org/10.1023/A:1019129717644

[17] Kuznetsov, A. (2013). On the convergence of the Gaver–Stehfest algorithm. *SIAM Journal on Numerical Analysis*, *51*(6), 2984–2998. https://doi.org/10.1137/13091974X

[18] Moorthy, M. V. (1995). Inversion of the multi-dimensional Laplace transform-expansion by Laguerre series. *Zeitschrift für angewandte Mathematik und Physik*, *46*(5), 793–806. https://doi.org/10.1007/BF00949080

[19] Smolyak, S. A. (1963). Quadrature and interpolation formulas for tensor products of certain classes of functions. *Doklady Akademii Nauk SSSR*, *148*(5), 1042–1045 (in Russian). https://www.mathnet.ru/eng/dan27586.

[20] Stehfest, H. (1970). Algorithm 368: Numerical inversion of Laplace transforms [D5]. *Communications of the ACM*, *13*(1), 47–49. https://doi.org/10.1145/361953.361969

[21] Trefethen, L. N., & Weideman, J. A. C. (2014). The exponentially convergent trapezoidal rule. *SIAM Review*, *56*(3), 385–458. https://doi.org/10.1137/130932132

[22] Weeks, W. T. (1966). Numerical inversion of Laplace transforms using Laguerre functions. *Journal of the ACM*, *13*(3), 419–429. https://doi.org/10.1145/321341.321351

[23] Weideman, J. A. C. (1999). Algorithms for parameter selection in the Weeks method for inverting the Laplace transform. *SIAM Journal on Scientific Computing*, *21*(1), 111–128. https://doi.org/10.1137/S1064827596312432

[1] Department of Mathematics, Amman Arab University, Amman, Jordan.
Email address: m.almomani@aau.edu.jo

[2] Department of Mathematics, Isra University, Amman, Jordan.
Email address: bahaabugazaleh@gmail.com